Mitochondrial ROS Induced Lysosomal Dysfunction and Autophagy Impairment in an Animal Model of Congenital Hereditary Endothelial Dystrophy

Rajalekshmy Shyam,[1] Diego G. Ogando,[1] Moonjung Choi,[1] Paloma B. Liton,[2] and Joseph A. Bonanno[1]

[1]Vision Science Program, School of Optometry, Indiana University, Bloomington, Indiana, United States
[2]Department of Ophthalmology, Duke University, Durham, North Carolina, United States

Correspondence: Rajalekshmy Shyam, Vision Science Program, School of Optometry, Indiana University, 800 E. Atwater Avenue, Bloomington, IN 47405, USA; rashyam@iu.edu.

Received: March 31, 2021
Accepted: August 18, 2021
Published: September 17, 2021

Citation: Shyam R, Ogando DG, Choi M, Liton PB, Bonanno JA. Mitochondrial ROS induced lysosomal dysfunction and autophagy impairment in an animal model of congenital hereditary endothelial dystrophy. *Invest Ophthalmol Vis Sci.* 2021;62(12):15. https://doi.org/10.1167/iovs.62.12.15

Purpose. The *Slc4a11* knock out (KO) mouse model recapitulates the human disease phenotype associated with congenital hereditary endothelial dystrophy (CHED). Increased mitochondrial reactive oxygen species (ROS) in the *Slc4a11* KO mouse model is a major cause of edema and endothelial cell loss. Here, we asked if autophagy was activated by ROS in the KO mice.

Methods. Immortalized cell lines and mouse corneal endothelia were used to measure autophagy and lysosome associated protein expressions using Protein Simple Wes immunoassay. Autophagy and lysosome functions were examined in wild type (WT) and KO cells as well as animals treated with the mitochondrial ROS quencher MitoQ.

Results. Even though autophagy activation was evident, autophagy flux was aberrant in *Slc4a11* KO cells and corneal endothelium. Expression of lysosomal proteins and lysosomal mass were decreased along with reduced nuclear translocation of lysosomal master regulator, transcription factor EB (TFEB). MitoQ reversed aberrant lysosomal functions and TFEB nuclear localization in KO cells. MitoQ injections in KO animals reduced corneal edema and decreased the rate of endothelial cell loss.

Conclusions. Mitochondrial ROS disrupts TFEB signaling causing lysosomal dysfunction with impairment of autophagy in *Slc4a11* KO corneal endothelium. Our study is the first to identify the presence as well as cause of lysosomal dysfunction in an animal model of CHED, and to identify a potential therapeutic approach.

Keywords: congenital hereditary endothelial dystrophy (CHED), mTOR, transcription factor EB (TFEB), lysosome, autophagy, MitoQ, reactive oxygen species (ROS), vATPase

The corneal endothelium is a monolayer on the posterior corneal surface facing the anterior chamber of the eye. These nonregenerating cells maintain corneal hydration and transparency through primary and secondary active transport processes.[1–3] The energy needed for this process is derived from a high density of mitochondria. Corneal endothelial diseases, such as Fuchs endothelial corneal dystrophy (FECD) and congenital hereditary endothelial dystrophy (CHED), are associated with dysfunctional mitochondria, increased reactive oxygen species (ROS), alterations in cell morphology, function, and eventually cell death.[4–7] Corneal edema is the main clinical manifestation of FECD and CHED,[8,9] and corneal transplantation is the only available treatment option. Although CHED is a rare recessive disorder, FECD affects nearly 4% of people over the age of 40 years and accounts for one-third of corneal transplants per year in the United States.[8–11]

Corneal endothelial cells highly express SLC4A11, an electrogenic NH_3 sensitive H^+ transporter, that is located in the basolateral membrane[11] and multiple cytoplasmic locations[12] including the inner mitochondrial membrane.[6] Homozygous recessive mutations in this gene are linked to early-onset CHED,[13] whereas heterozygous mutations are implicated in later life FECD.[14] The *Slc4a11* knockout (KO) mouse model recapitulates the disease progression of CHED along with increased corneal endothelial oxidative stress,[15,16] a well-known characteristic of corneal endothelial dystrophies.[6,7] Recent work from our laboratory demonstrated that Slc4a11 is an ammonia-sensitive mitochondrial uncoupler. The absence of *Slc4a11* causes glutamine-induced excessive mitoROS production, deficient ATP production, and eventual apoptosis.[6] Although endothelial cell function and morphology are affected early in the mouse model, cell loss is not initially apparent but progresses over many weeks.[15] Mitochondrial ROS can lead to increased autophagy, which in certain cell types helps in survival.[17] Whether autophagy is activated by *Slc4a11* loss of function and is instrumental in slowing cell death in the corneal endothelium are unknown.

In the current project, we examined the autophagy process in corneal endothelial cells lacking Slc4a11 and found that while autophagy is activated, it is aberrant. We

found that autophagy flux is disrupted in both a *Slc4a11* KO corneal endothelial cell line and mouse endothelial tissue, primarily due to lysosome dysfunction. Quenching mitochondrial ROS with MitoQ rescued lysosomal function and autophagy flux. Moreover, MitoQ slowed the development of corneal edema in the *Slc4a11* KO mouse and reduced endothelial cell loss, while improving autophagy and lysosome protein expression. These findings provide further evidence that mitochondrial Slc4a11 modulates ROS production that if quenched can slow the progression of corneal edema in a mouse model of CHED.

Materials and Methods

Animal Model

Slc4a11 wild-type (WT) and KO mice[15] were housed and maintained in pathogen-free conditions and used in the experiments in accordance with institutional guidelines and the current regulations of the National Institutes of Health, the United States Department of Health and Human Services, the United States Department of Agriculture, and the Association for Research in Vision and Ophthalmology (ARVO) Statement for the Use of Animals in Ophthalmic and Vision Research. *Slc4a11* KO mice were created with a targeted deletion of exons 9–13 of the mouse *Slc4a11* gene.[15]

Cell Culture Experiments

The generation of conditionally immortalized mouse corneal endothelial cells (MCEC) $Slc4a11^{+/+}$ and $Slc4a11^{-/-}$ is described previously.[18] Cells were cultured in Complete Media, which contains OptiMEM-I medium (#51985; Thermo Fisher Scientific, Canoga Park, CA, USA), 14 mM glucose and 4 mM L-alanyl glutamine supplemented with 8% heat-inactivated fetal bovine serum (FBS; #10082139; Thermo Fisher Scientific), epidermal growth factor (EGF) 5 ng/mL (#01-107; Millipore, Darmstadt, Germany), pituitary extract 100 µg/mL (Hyclone 15 Laboratories, Logan, UT, USA), calcium chloride 200 mg/L, 0.08% chondroitin sulfate (#G6737; SigmaAldrich Corp., St. Louis, MO, USA), gentamicin 50 µg/mL (#15710072; Thermo Fisher Scientific), antibiotic/antimycotic solution diluted 1:100 (#15240062; Thermo Fisher Scientific) and 44 units/mL IFN-γ (#485-MI; R&D Systems, Minneapolis, MN, USA).

For the experiments, cells were incubated in Assay Media, which contained Earle's Balanced Salt Solution supplemented with 5.5 mM glucose (#141553; Thermo Fisher Scientific), 0.5 mM glutamine (#250030-081; Thermo Fisher Scientific), and 0.5% dialyzed FBS (#26400-036; Thermo Fisher Scientific) at 33°C for 16 hours. Drug treatments, 50 nM BafilomycinA1 (#SML1661; SigmaAldrich Corp.), 2 µM MitoQ (#317102; Medkoo Biosciences, Morrisville, NC, USA) were added into the assay media for 16 hours.

Transient Transfection

Mouse corneal endothelial cell (MCEC) WT and KO cells were grown on glass coverslips. Using Lipofectamine 3000 (L3000001; Thermo Fisher Scientific), following manufacturer's instructions, cells were transfected with pMRX-IP-GFP-LC3-RFP-LC3ΔG (#84572; Addgene). Then, 72 hours post transfection, the cells were subject to treatment in assay media for 16 hours. Following this, the cells were fixed with 4% paraformaldehyde for 5 minutes, permeabilized using 0.1% Triton X-100 for 5 minutes, and blocked using 3% BSA for 1 hour. Primary antibody incubation using 1:100 anti-GFP (#sc-9996; Santa Cruz Biotechnology, Dallas, TX, USA) and 1:100 anti-RFP (#600-401-379; Rockland Immunochemicals, Gilbertsville, PA, USA) was conducted over night at 4°C. Following secondary antibody incubation, and washes, the cells were mounted using prolong gold antifade mounting media (P36930; Thermo Fisher Scientific) and examined by Zeiss LSM 800 confocal microscope (Zeiss, Oberkochen, Germany) using 63X oil objective.

Western Blot Analysis

Protein lysates were prepared using 1X RIPA analysis (10X RIPA buffer, #9806; Cell Signaling Technologies, Danvers, MA, USA) containing protease and phosphatase inhibitors (#5872S; Cell Signaling Technologies). Protein concentration was measured using BCA assay (#23227; Thermo Fisher Scientific), and 20 µg of proteins were resolved by either 8% SDS-PAGE or 15% for lower molecular weights, transferred onto Nitrocellulose membrane (#1620115; BioRad, Hercules, CA, USA), blocked using 5% milk in TBST for 1 hour followed by primary antibody incubation at 4°C for overnight. Secondary antibody incubation was carried out for an hour at room temperature, and the blots were imaged using BioRad ChemiDoc imaging system. Antibodies used only in traditional Western Blots are – LC3b (#2775; Cell Signaling Technologies), and β-actin (#A5441; Thermo Fisher Scientific).

Protein Simple – Simple Western Wes Immunoassay for Protein Expression

Corneas were dissected and the endothelial cell layer was removed by peeling Descemet's membrane with jeweler's forceps. Protein lysates from corneal endothelial layers were pooled from two animals, lysed in radioimmunoprecipitation (RIPA) lysis buffer containing protease and phosphatase inhibitors. Equal amounts of protein (1–3 µg) were loaded into 12 to 230 kDa separation module kit, and analyzed using the Protein Simple Wes System (Protein Simple, San Jose, CA, USA) following the manufacturer's instructions. Wes data are obtained as virtual blots in which the molecular weight and signal intensity are presented. Results in the form of electropherograms are also obtained with this approach. Molecular weights associated with the bands are presented and the area under the curve in these plots correspond to the chemiluminescence intensities. Table 1 includes antibodies used in the Wes system. Traditional Western Blot was performed for LC3b because LC3bI and LC3bII bands were not properly resolved with Wes immunoassay.

Real Time PCR

Total RNA from MCEC WT and KO cells was isolated using RNA mini kit (#74104; Qiagen, Germantown, MD, USA). The, 1 µg of RNA was used to prepare cDNA using a high-capacity RNA to the DNA kit (#4388950; Thermo Fisher Scientific). The National Center for Biotechnology Information (NCBI) primer designing tool was used to design all other primers used for this study. The primers used in this study can be found in Table 2. Real time PCR was conducted using SYBR green dye using a BioRad CFX96 system. Relative quantitation was performed using $2^{-\Delta\Delta Ct}$ method against

Investigative Ophthalmology & Visual Science

Table 1. List of Antibodies Used for Traditional Western Blot and Wes Immunoassay

Antibody Name	Catalog Number, and Company	Dilution for Wes Immunoassay	Dilution for Western Blot
mTOR	#2983S, Cell Signaling Technologies	1:50	Not used
Phospho-mTOR	#5536S, Cell Signaling Technologies	1:10	Not used
P62	# 23214, Cell Signaling Technologies	1:10	1:1000
Atg5	#12994, Cell Signaling Technologies	1:10	Not used
LC3b	#2775, Cell Signaling Technologies	Not used	1:1000
β-actin	#A5441, Thermo Fisher Scientific	Not used	1:2500
α-tubulin	#690, Novus Biologicals	1:50	Not used
v-ATPase	#14617S, Cell Signaling Technologies	1:10	Not used
Cathepsin B	#31718, Cell Signaling Technologies	1:10	1:1000
TFEB	# 13372-1-AP, Proteintech	1:10	Not used
TFEB	# 32361, Cell Signaling Technologies	1:10	Not used
Lamin A/C	# 4777, Cell Signaling Technologies	1:10	Not used
GAPDH	#5174, Cell Signaling Technologies	1:50	Not used

Table 2. Primers Used in Real Time PCR Experiment

Bloc1s1 - Forward	GGTGAGCCAAGGCATAGTCC
Bloc1s1 - Reverse	GAGGTGATCCACCAACGCTT
Gabarap - Forward	GCTGAGCTAGTGGCGTATGT
Gabarap - Reverse	CGGATTTTCTCGCCCTCAGA
Atp6v0b - Forward	GGTCGTTGTGGGAATCTGCT
Atp6v0b - Reverse	CATAGATGGCCACCGCTTCA
Atp6v0c - Forward	TGGTGCCAGGGCCCATAAAT
Atp6v0c - Reverse	CTCCTGTAGAGGGTGATGCC
Gla - Forward	TTGGGGTCAGAGCATTGGAC
Gla - Reverse	TTGCGAGGTGTTTGATCCCA
Ctsb - Forward	ACCTGTAACTGCTCACACCT
Ctsb - Reverse	GCTCCCTGTTCCCTTTGAACT
Ctsd - Forward	CAACGTGCTTCCGGTCTTTG
Ctsd - Reverse	CTCATTGCCCACCTCCAACT
Lamp1 - Forward	AGCATACCGGTGTGTCAGTG
Lamp1 - Reverse	AGGCAGGTTCCGTTGTTACC

housekeeping gene. Fold change (FC) is calculated as $2^{-\Delta\Delta CT}$. Data is plotted on Log_{10} scale.

Nuclear and Cytosolic Extraction

MCEC WT and KO cells were treated in assay media for 16 hours. Nuclear and cytosol extraction was carried out using a Nuclear Extraction kit (#ab113474; Abcam, Cambridge, UK) following the manufacturer's instructions. Protein concentration was determined using the Bradford assay (#ab102535; Abcam). Equal amounts of cytosolic fractions (approximately 1.5% of total cytosol extract), and equal amounts of nuclear fractions (approximately 15% of the total extract) were loaded to perform Wes immunoassay using antibodies against transcription factor EB (TFEB). Lamin A/C and GAPDH were used as nuclear and cytoplasm references, respectively. Antibody information and dilutions are indicated in Table 1.

Immunofluorescence

Mouse corneas were isolated, and washed in ice cold PBS. Following fixation in 4% paraformaldehyde for 10 minutes, the tissues were permeabilized using 0.5% Triton X-100 for 10 minutes, blocked using 3% Donkey Serum for 1 hour, and incubated in primary antibody containing LC3b (#2775; Cell Signaling Technologies) for overnight at 4°C, followed by secondary antibody incubation for 1 hour at room temperature. The corneas were cut radially, and mounted for imaging. LAMP1 staining on MCEC was conducted using the above-mentioned immunofluorescence protocol. Lamp 1 antibody (#DDX0191P; Novus Biologicals, 1:200) was used for this purpose. Images were acquired for LC3b and Lamp1 staining using the Zeiss LSM 800 confocal microscope.

Cathepsin L Activity

Cathepsin L activity was measured on fresh corneal cups using the Magic Red Cathepsin L assay kit (#941; Immunochemistry Technologies, Bloomington, MN, USA) following the manufacturer's instructions. Magic Red staining images were acquired on the Zeiss 15 Apotome microscope. Magic Red reagent enters the cells in a non-fluorescent state. When cleaved by Cathepsin, it emits fluorescence.

Live Cell Imaging

MCEC WT and KO cells were grown in 8-well Nunc Lab-Tek II CC2 chamber slides (Thermo Fisher Scientific), treated with assay media for 16 to 18 hours. Then, 1 µM Lysosensor Green DND-189 (L7535; Thermo Fisher Scientific) or 150 nM Lysotracker Red DND-99 (L7528; Thermo Fisher Scientific) was added, and the cells were incubated at 37°C for 5 minutes. Following a brief wash with PBS, cells were mounted using a glass coverslip and imaged at 63X using the Zeiss LSM 800 confocal microscope.

Quantification of Confocal Fluorescence Images

Images for each experiment were acquired with the same settings. Fluorescence microscopy images were analyzed and fluorescence intensity quantified using ImageJ (US National Institutes of Health, Bethesda, MD, USA). At least 35 cells were outlined for each condition, and cells were counted from eight or more images. Experiments were repeated on three different samples, and background intensities were measured by outlining a cell free region in the image, and subtracting this from the fluorescence intensity measurement of the cells. The resultant value was considered the mean fluorescence intensity.

Corneal Thickness Measurement

Corneal cross-section images were obtained in vivo using an iVue Optical Coherence Tomographer (OCT; Optovue,

Investigative Ophthalmology & Visual Science

Fremont, CA, USA). All corneal thickness measurements were made at the same time of day. At least three central corneal thickness measurements were made for each eye and averaged. Central corneal thickness measurements were made using horizontal line scans. Eight scans were obtained for each eye, and these values were averaged to get a final image, which was then used to calculate the thickness. Using a distance tool included in the software at the corneal apex, we measured the corneal thickness.

The OCT operator was blinded to the experimental condition.

MitoQ Injections

MitoQ (#317102; Medkoo Biosciences) was dissolved in equal amount of ethanol: distilled sterile water to obtain a final concentration of 1 mM. Then, 100 µL of the above solution containing 68 µg of MitoQ was intraperitoneally injected into the animals on alternate days for 4 weeks at the same time each day. Control animals were injected with equal volumes of vehicle at the same time/day for the same duration. Animals were monitored for any changes in health or behavior during the experiment duration. All animals were provided with vet-approved supplements; peanut butter or Bacon Softies (Bio-Serv, Flemington, NJ, USA) for the duration of the treatment to prevent stress-induced weight loss due to increased handling. All analyses of corneal thickness following the MitoQ injections were blinded.

MitoSox Staining

Whole corneas were dissected and mounted with the endothelium facing up in small plastic dishes. A volume of 10 µl of 1 mM MitoSox (#M36008; Thermo Fisher Scientific) was added on the endothelial side and incubated at room temperature for 30 minutes. The corneas were washed 3 times for 5 minutes each with 10 µl of 1X PBS. After removing all liquid, corneas were positioned in wells of 96-well plate and Fluorescence (excitation = 510 nm, emission = 580 nM) was measured in a microplate reader.

Statistical Analysis

All experiments were performed at least three times on different days. Error bars represent mean ± SD. Statistical significance was calculated using unpaired *t*-tests when two groups were involved. ANOVA with Tukey's multiple comparisons test was used to determine statistical significance if more than two groups were analyzed. Statistical analyses were conducted using Graph Pad Prism software (La Jolla, CA, USA).

Model Figures

The model figures were created with the aid of BioRender.com.

Results

Impaired Autophagy Flux in Slc4a11 KO Corneal Endothelial Cells and Tissue

Using immortalized MCECs established from *Slc4a11* WT and KO mice,[18] we first asked if autophagy is activated. Increased autophagy is often triggered by a decrease in phosphorylated mechanistic target of rapamycin (mTOR). This stimulates phagophore formation which in turn matures into an autophagosome and eventually fuses with lysosomes resulting in the degradation of its components as summarized in Figure 1A.

Because of the small amount of protein in mouse corneal endothelial samples (approximately 8 µg/pair of eyes), we used a capillary electrophoresis immunoassay approach (Protein Simple Simple Western Wes) for all in vivo samples and some in vitro samples, as indicated. This approach accommodates 1 to 3 µg of total protein to obtain quantifiable western blot like results.[19–22] Figures 1B and 1C show that the p-mTOR/mTOR ratio was decreased in *Slc4a11* KO compared to WT cells. Traditional Western blots indicate the ratio of microtubule associate protein 1A/1B Light chain 3 (LC3bII/I) was increased (see Figs. 1B, 1C), suggesting that the initial steps of autophagy are activated in KO cells relative to WT. LC3bI and II refer to the non-lipidated and lipidated forms of LC3b. LC3bII is recruited to the autophagosome membrane during the expansion and fusion. Detecting the conversion of LC3bI (approximately 19 KDa) to LC3bII (approximately 17 KDa) is considered to be an indicator of autophagy in mammalian cells. P62, a marker of autophagy flux that is part of the phagosome, is typically low during activated autophagy (due to degradation), however, in *Slc4a11* KO cells P62 was elevated (see Figs. 1B, 1C). In cells with normal autophagy flux, treatment with Bafilomycin A1 (BafA1), which blocks vacuolar H^+-ATPase activity, alkalinizes lysosomes and increases the accumulation of autophagy related proteins (see Fig. 1A). In WT cells, BafA1 increased the protein levels of autophagy related 5 (Atg5) and P62. The LC3bII/I ratio (see Figs. 1B, 1C) was increased in WT cells with BafA1 treatment as expected. In the KO cells with BafA1 treatment, the ratio of LC3bII/I remained similar to those observed in KO cells. BafA1 had no effect on P62 levels in KO cells. We observed a slight reduction in Atg5 level in the KO cells with or without BafA1, but this was not significant. Taken together, these results suggest compromised autophagy flux in *Slc4a11* KO MCEC.

Autophagy flux was also measured in MCEC WT and KO cells by confocal imaging following transfection with pMRX-IP-GFP-LC3-RFP-LC3ΔG, a fluorescent probe of autophagy flux[23] (Supplementary Fig. S1). The c-terminus of the LC3 construct is cleaved by Atg4, an autophagy initiation factor. This results in the production of GFP-LC3 and RFP-LC3ΔG. GFP-LC3 is degraded in the lysosomes upon autophagy, whereas RFP-LC3ΔG remains cytosolic (see Supplementary Fig. S1A). Autophagy flux is assessed by comparing the GFP/RFP ratio. In the KO cells (Supplementary Figs. S1B, S1C), the GFP/RFP ratio was two-fold higher than that of the WT cells. Consistent with the Western blot results, BafA1 caused an increased GFP/RFP ratio in WT cells (see Supplementary Figs. S1B, S1C), whereas in KO cells the ratio did not change.

We then measured autophagy in the *Slc4a11* KO mouse corneal endothelial tissue from 10-week-old KO animals. A two-fold increase in LC3 puncta numbers (Figs. 1D, 1E) was observed. Moreover, increased expression of P62 and decreased levels of p-mTOR/mTOR ratio were found in the KO animal tissue when compared to age matched WT controls (Figs. 1F, 1G). These results parallel the in vitro findings confirming that autophagy is activated, but dysregulated in *Slc4a11* KO corneal endothelium in vivo.

Investigative Ophthalmology & Visual Science

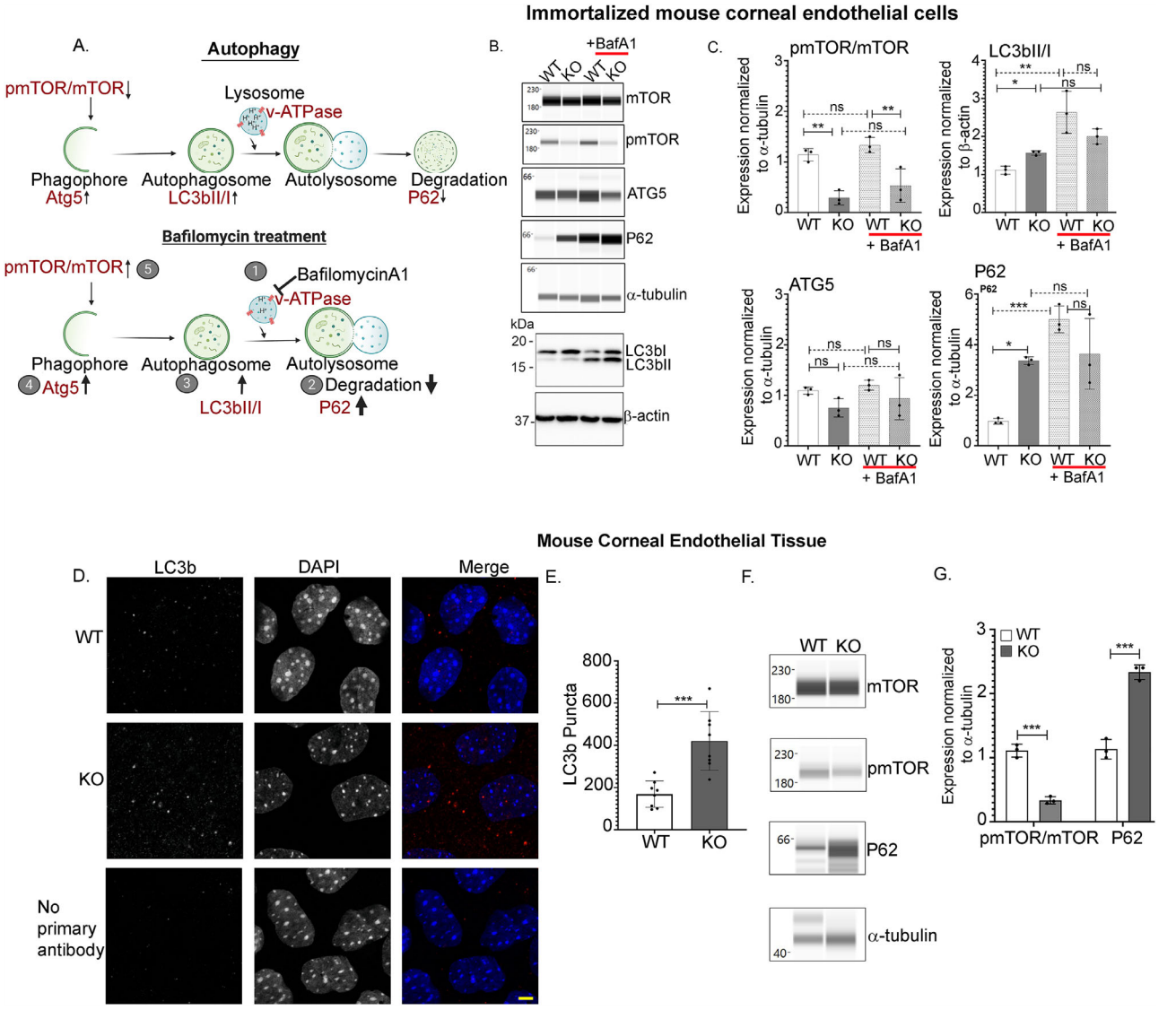

Figure 1. Autophagy flux is aberrant in *Slc4a11* KO corneal endothelial cells. (**A**) In basal autophagy, autophagosome formation occurs followed by fusion with lysosomes and the degradation of substrates. In BafilomycinA1 (BafA1) treated cells (1), the lysosomal proton pump (v-ATPase), which is responsible for its acidic environment is inactivated. This leads to the accumulation of non-degraded autophagy substrates in the cell (2), which further increases the levels of proteins involved in autophagosome (3), and phagophore formation (4), which eventually increases pmTOR/mTOR ratio (5). (**B**) Wes immunoassay for p-mTOR (Ser 2448), mTOR, Atg5, P62 in *Slc4a11* WT and KO MCEC (± 50 nM BafA1). Western Blot of the same lysates were probed for LC3b and β-actin. (**C**) Quantification of panel **B** data, mean ± SD. ***$P < 0.001$, **$P < 0.01$, *$P < 0.05$, ns = not significant (1-way ANOVA with Tukey's multiple comparisons test). (**D**) Immunofluorescence of corneal endothelial tissue from *Slc4a11* WT and KO mice for LC3b (*red*) counterstained with DAPI (*blue*). Scale bar – 5 µm. (**E**) Quantification of LC3b puncta from panel **D** data, mean ± SD, ***$P < 0.001$ (Student's *t*-test). (**F**) Wes immunoassay of mTOR, pmTOR (Ser 2448) and P62 from *Slc4a11* WT and KO corneal endothelial tissues. (**G**) Quantification of data from panel **F**, mean ± SD. ***$P < 0.001$ (Student's *t*-test, $n = 3$).

Evidence of Lysosomal Dysfunction in Slc4a11 KO Corneal Endothelial Cells

Active lysosomes are essential for the ultimate degradation of autophagy substrates. With the observation of decreased autophagy flux in KO MCEC, we investigated lysosomal function. We evaluated expression of Vacuolar ATPase (v-ATPase), which is involved in lysosomal acidification, and lysosomal hydrolase, Cathepsin B. Wes immunoassay analyses indicate decreased v-ATPase and Cathepsin B expression in KO MCEC (Figs. 2A, 2B). Maturation of Cathepsin B requires an acidic lysosome lumen.[24,25] To validate the Wes results, BafA1 treatment eliminated mature Cathepsin B detection in WT and KO cells indicating higher lysosomal pH as a potential cause for the reduction in Cathepsin B levels.

Next, we examined lysosomal protein expression in corneal endothelial tissue of *Slc4a11* KO animals. We observed a reduction in the expression of lysosomal proteins, v-ATPase and Cathepsin B (Figs. 2C, 2D), consistent with the observations in MCEC. Cathepsin L activity was measured with Magic Red. Our data shows decreased levels

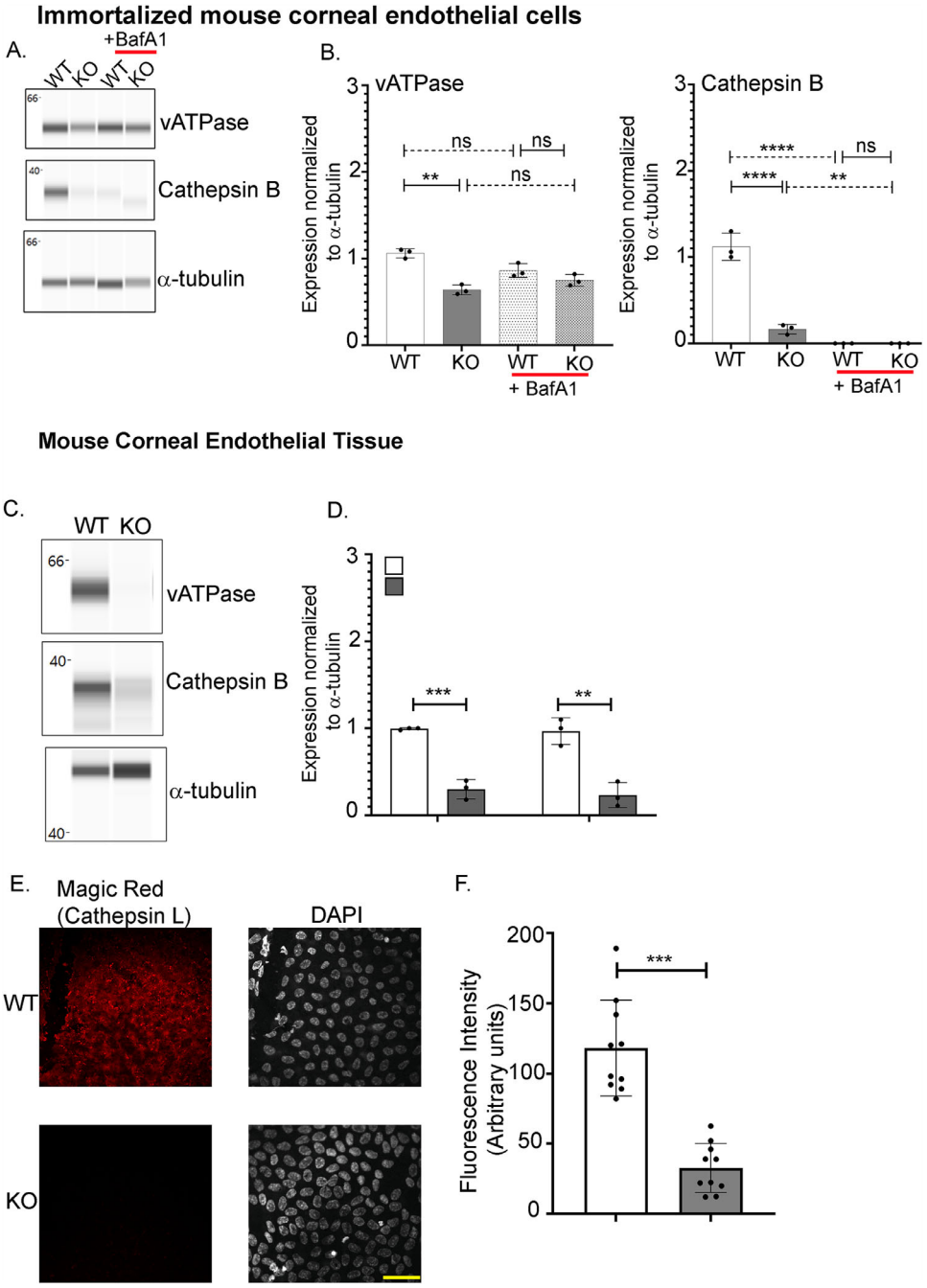

Figure 2. Lysosomal dysfunction is evident in *Slc4a11* KO corneal endothelial cells. (**A**) Wes immunoassay of v-ATPase, and Cathepsin B using *Slc4a11* WT and KO MCEC whole cell lysates (± 50 nM BafA1). (**B**) Quantification of data from panel **A**, $n = 3$, mean ± SD. $^{**}P < 0.01$, $^{***}P < 0.001$, $^{****}P < 0.0001$, ns = not significant (1-way ANOVA with Tukey's multiple comparisons test). (**C**) Wes immunoassay of v-ATPase, and Cathepsin B from corneal endothelium of*Slc4a11* WT and KO mice. (**D**) Quantification of panel **C** data, $n = 3$, mean ± SD. $^{***}P < 0.0001$, $^{**}P < 0.01$ (Student's *t*-test). (**E**) Magic Red assessment of Cathepsin L activity in *Slc4a11* WT and KO corneal endothelial tissue. Scale bar – 50 µm. (**F**) Quantification of Magic Red fluorescence, $n = 5$, mean ± SD. $^{****}P < 0.0001$ (Student's *t*-test).

of Magic Red fluorescence in the KO tissue when compared to age matched WT controls (Figs. 2E, 2F) confirming deficient lysosomal activity.

To assess whether the decrease in lysosomal activities were a result of decreased lysosomal content, MCEC were stained with Lysotracker Red, a dye that selectively binds to acidic organelles. Decreased lysosomal mass was seen in *Slc4a11* KO cells when compared to WT cells (Figs. 3A, 3B). These results were corroborated by immunostaining of Lysosomal associated membrane protein 1 (Lamp1; see Supplementary Figs. S2A, S2B). In addition, lysosomal pH determined by LysoSensor Green staining was significantly diminished in *Slc4a11* KO cells compared to WT (Figs. 3C, 3D). Cells treated with BafA1 were used as positive control.

Investigative Ophthalmology & Visual Science

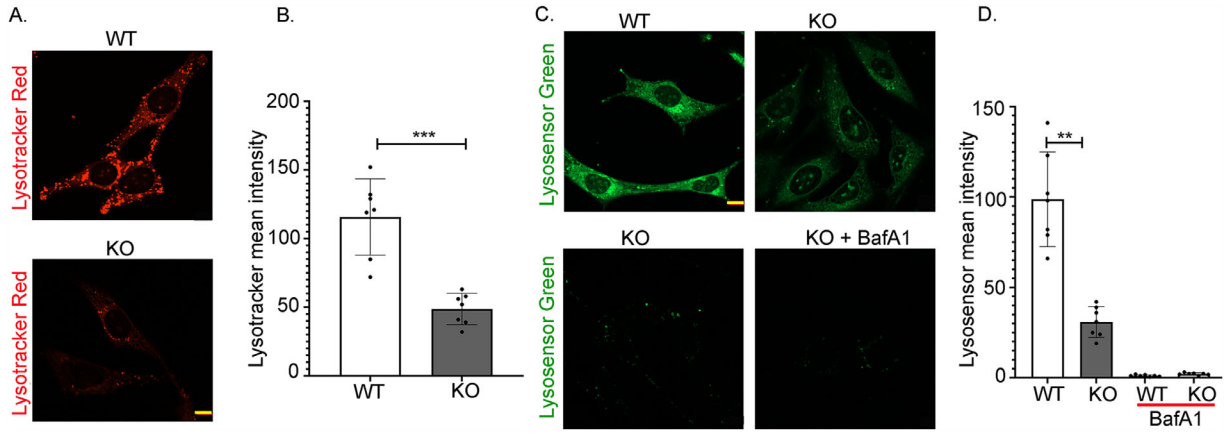

Figure 3. Lysosome mass and pH are affected in *Slc4a11* KO cells. (**A**) Lysotracker Red-DND 99 staining to visualize lysosomal mass in *Slc4a11* WT and KO MCEC. Scale bar – 10 µM. (**B**) Quantification of fluorescence intensities from panel **A**. Mean fluorescence intensities were measured using ImageJ. Twenty-five cells from seven images were used for this analysis ($n = 7$). Mean ± SD. ****$P < 0.0001$ (Student's *t*-test). (**C**) Lysosomal pH (Lysosensor Green-DND 189) staining of Slc4a11 WT and KO MCEC. Scale bar – 10 µm. (**D**) Quantification of the fluorescence intensities from panel **C**. Mean fluorescence intensities were measured using ImageJ. Forty cells from seven images were used for this analysis ($n = 7$). Mean ± SD. **$P < 0.01$ (1-way ANOVA with Tukey's multiple comparisons test).

TFEB Activities are Reduced in Slc4a11 KO Corneal Endothelial Cells

A major regulator of both autophagy and lysosomal function is TFEB. This protein is known to regulate lysosomal biogenesis, autophagy, lysosomal exocytosis, and macromolecular degradation in several cell types.[26–28] We therefore determined whether the expression and activities of TFEB are affected in *Slc4a11* KO. Nuclear and cytosolic extractions were conducted for Wes immunoassay-based detection of TFEB levels in *Slc4a11* WT and KO cells. Whereas TFEB was detected in cytosol and nucleus in WT cells, significant reductions in the nuclear TFEB levels (Figs. 4A, 4B) were observed in KO cells. TFEB regulates the transcription of several genes that in turn regulate lysosomal biogenesis, function, and autophagy. Consistent with the lack of TFEB activity, Figure 4C shows that a subset of these coordinated lysosomal expression and regulation (CLEAR) pathway genes,[29,30] were significantly downregulated in KO MCEC.

Owing to the minute amounts of protein that can be isolated from mouse corneal endothelial cells, cell fractionation procedures were not possible. Therefore, we conducted Wes immunoassay to detect total TFEB levels in the corneal endothelia of *Slc4a11* WT and KO animals. Because TFEB is known to regulate its own transcriptional activation,[26] a decrease in total TFEB levels in the tissue lysate would be indicative of the decreased transcriptional activity of this protein. In the tissue lysates, TFEB expression was significantly reduced in the KO (Figs. 4D, 4E).

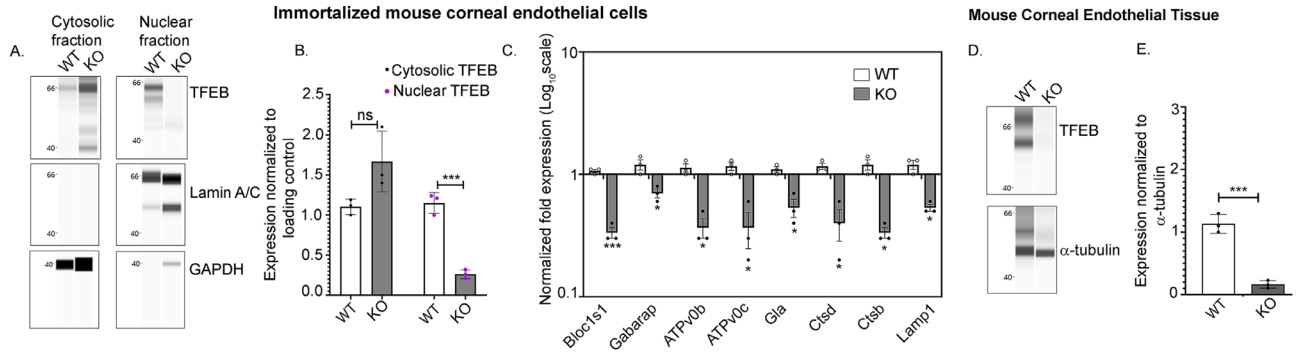

Figure 4. Deficient TFEB nuclear translocation in *Slc4a11* KO cells. (**A**) Wes immunoassay of TFEB, Lamin A/C, and GAPDH in nuclear and cytosolic extracts from *Slc4a11* WT and KO MCEC. Nuclear membrane proteins, Lamin A/C, and cytoplasmic protein, Glyceraldehyde 3-phosphate dehydrogenase (GAPDH) were used as loading control for the respective fractions and also to rule out cross-contamination between the fractions. (**B**) Quantification of Wes results from panel **A**. Mean ± SD. ***$P < 0.001$. ns = not significant (Student's *t*-test). (**C**) Q-PCR of a subset of TFEB regulated CLEAR network genes in *Slc4a11* WT and KO MCEC. Blocs1 – Biogenesis of Lysosomal Organelles Complex 1 Subunit 1, Gabarap - GABAA receptor-associated protein 1, Atpv0b – vATPase subunit b, Atpv0c – vATPase subunit C, Gla –Alpha galactosidase A , Ctsd – Cathepsin D, Ctsb- Cathepsin B, and Lamp1- Lysosome-associated membrane glycoprotein 1. Expression normalized to β-actin, *$P < 0.05$, ***$P < 0.001$ (Student's *t*-test). (**D**) Wes immunoassay of TFEB from *Slc4a11* WT and KO corneal endothelial tissue. (**E**) Quantification of panel **D** data, mean ± SD, ***$P < 0.0001$, $n = 3$ (Student's *t*-test).

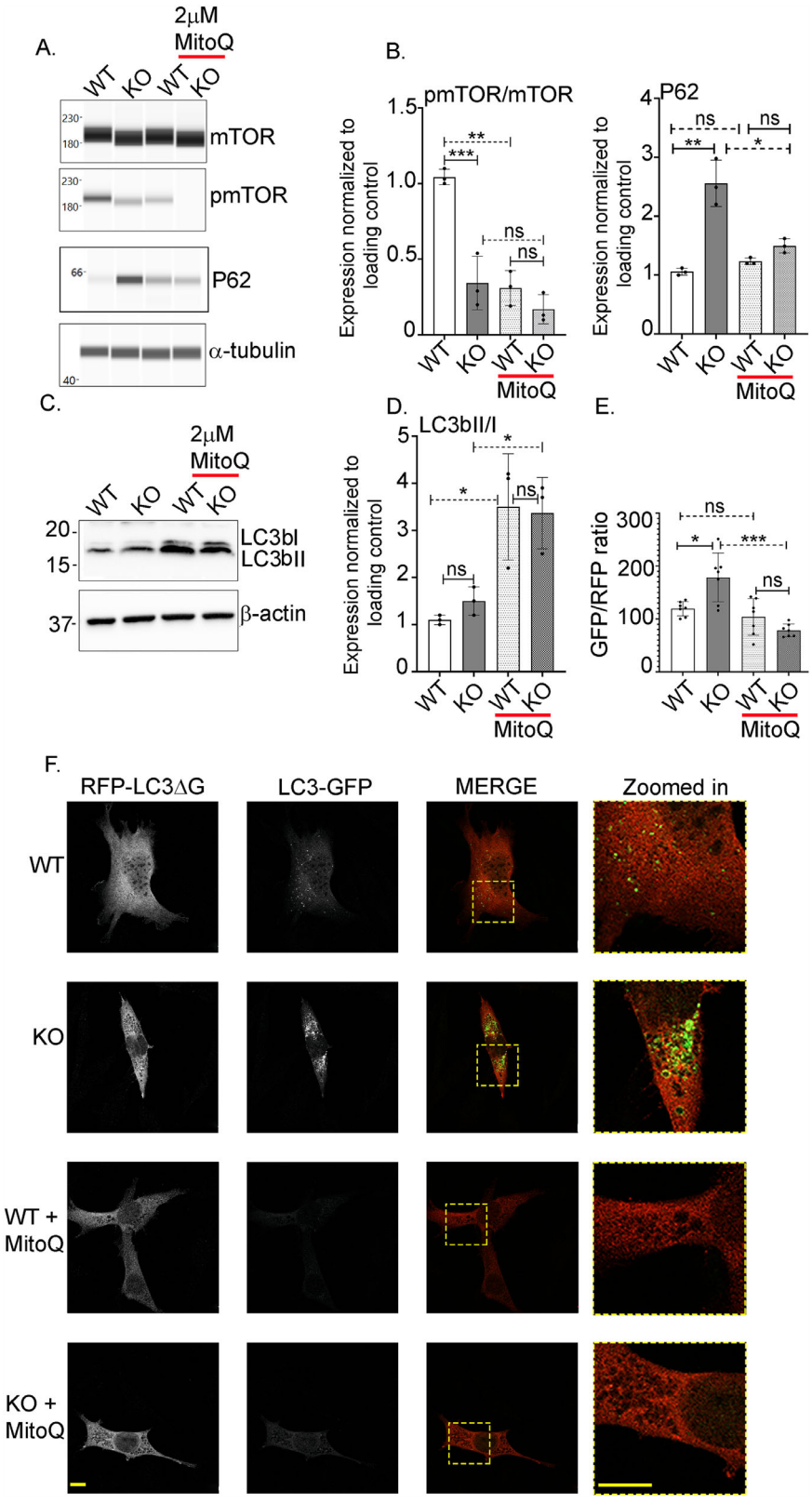

Figure 5. MitoQ improves autophagy *Slc4a11* KO cells. (**A**) Wes immunoassay of pmTOR, mTOR, and P62 from *Slc4a11* WT and KO MCEC ± MitoQ. (**B**) Quantification of panel **A** data, $n = 3$. (**C**) Western Blots of LC3b and β-actin in *Slc4a11* WT and KO MCEC ± MitoQ. (**D**) Quantification of panel **C** data, $n = 3$. (**E**, **F**) Detection of GFP and RFP fluorescence ratio in *Slc4a11* WT, KO (± MitoQ) MCEC transfected with GFP-LC3-RFP-LC3ΔG and Quantification. Scale bar – 10 μm, $n = 7$. *$P < 0.05$, **$P < 0.01$, ***$P < 0.001$, ****$P < 0.0001$, mean ± SD (1-way ANOVA with Tukey's multiple comparisons test).

Investigative Ophthalmology & Visual Science

Treatment With Mitochondrial ROS Quencher, MitoQ, Reverses Autophagy Impairment, and Lysosomal Dysfunction in Slc4a11 KO Corneal Endothelial Cells

Our previous work has shown that Slc4a11 acts as an NH_3-sensitive mitochondrial uncoupler.[6] We found that in the presence of glutamine, *Slc4a11* KO mouse corneal endothelia produce significantly higher levels of mitochondrial superoxide and a greater rate of apoptosis. To determine whether glutamine affects autophagy and lysosomal functions in *Slc4a11* KO, cells were incubated in media with or without glutamine (Supplementary Figs. S3A, S3B). In the absence of glutamine, KO cells showed increased LC3bII/I ratio and decreased P62 levels compared to WT cells suggesting increased autophagy. In addition, BafA1 treatment in the absence of glutamine revealed the expected increase in LC3bII/I ratio (see Supplementary Figs. S3A, S3B). Expression of lysosomal acid hydrolase, Cathepsin B, was also evident in KO cells in the absence of glutamine compared to glutamine treatment (see Supplementary Figs. S3A, S3B). These data indicate that in *Slc4a11* KO cells, dysfunctional autophagy and lysosomal malfunctions (see Figs. 1–3) are attributable to glutamine.

Because glutamine induced mitochondrial ROS was found to be the major contributing factor for apoptosis and metabolic dysfunctions associated with the loss of *Slc4a11* in the corneal endothelium,[6] we asked whether quenching oxidative stress would improve autophagy and lysosomal dysfunctions in *Slc4a11* KO cells.[31,32] Our previous study[6] had shown that a mitochondria specific antioxidant MitoQ[31,32] can reduce mitochondrial ROS in corneal endothelium, and we confirmed that treatment with 2 µM MitoQ resulted in a significant mitoROS reduction in the KO MCEC (see Supplementary Figs. S4A, S4B). MitoQ treatment decreased pmTOR/mTOR as well as P62 levels (Figs. 5A, 5B). In addition, MitoQ increased the LC3bII/I ratio in KO cells (Figs. 5C, 5D) and decreased pMRX-IP-GFP-LC3-RFP-LC3ΔG, GFP/RFP ratio in KO comparable to WT cells (Figs. 5E, 5F).

Lysosomal function, as measured by v-ATPase, was increased in KO MCEC with MitoQ treatment (Figs. 6A, 6B). MitoQ diminished nuclear TFEB in WT, but rescued TFEB to nucleus in KO (Figs. 6C, 6D). Similarly, lysosomal mass (Figs. 6F, 6G) and pH (Figs. 6H, 6I) were improved by MitoQ. These data indicate that quenching mitochondrial ROS restores autophagy flux in the *Slc4a11* KO MCEC.

MitoQ Mediated Reduction of Disease Phenotypes Associated With CHED in Slc4a11 KO Animals

The major clinical features of CHED are progressive corneal edema and endothelial cell loss. The *Slc4a11* KO mouse model recapitulates these phenotypes (14). In this animal model, significant corneal edema is apparent at 8 weeks of age, and this continues to increase through adulthood. To

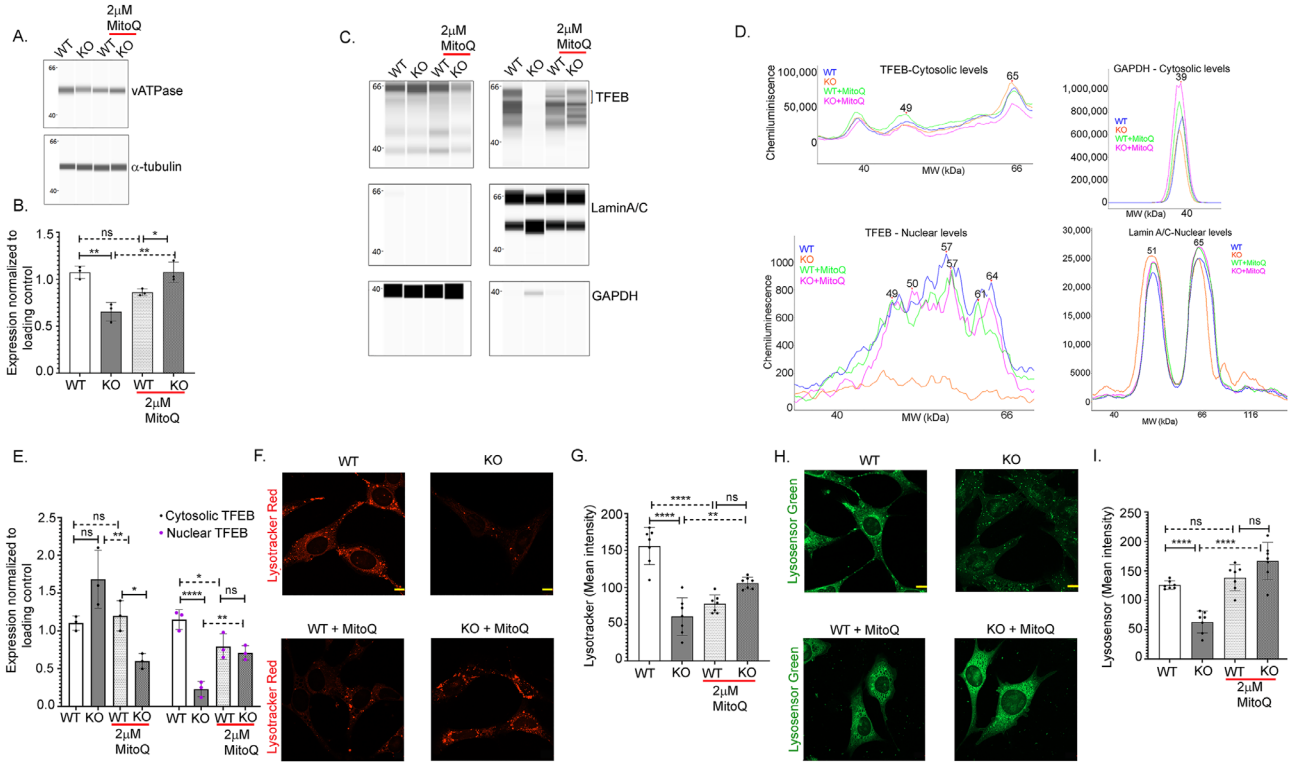

Figure 6. MitoQ improves lysosomal function in MCEC KO cells. (**A**) Wes immunoassay of v-ATPase from WT and KO *Slc4a11* MCEC ± MitoQ treatment. (**B**) Quantification of panel **A** data, $n = 3$. (**C**) Wes immunoassay of TFEB, Lamin A/C, and GAPDH from *Slc4a11* WT and KO MCEC cytosolic and nuclear fractions. (**D**) Electropherograms of Wes immunoassay from panel **C** showing the size and intensities of the bands in **C**. (**E**) Quantification of panel **C** data, $n = 3$. (**F**) Comparison of lysosome numbers (Lysotracker Red-DND 99) in *Slc4a11* WT and KO MCEC, scale bar – 10 µm. (**G**) Quantification of panel **F** data, $n = 7$. (**H**) Comparison of lysosomal pH (Lysosensor Green -DND 189) in *Slc4a11* WT and KO ± MitoQ, Scale bar – 10 µm. (**I**) Quantification of panel **H** data, $n = 7$. *$P < 0.05$, **$P < 0.01$, ***$P < 0.001$, ****$P < 0.0001$, mean ± SD (1-way ANOVA with Tukey's multiple comparisons).

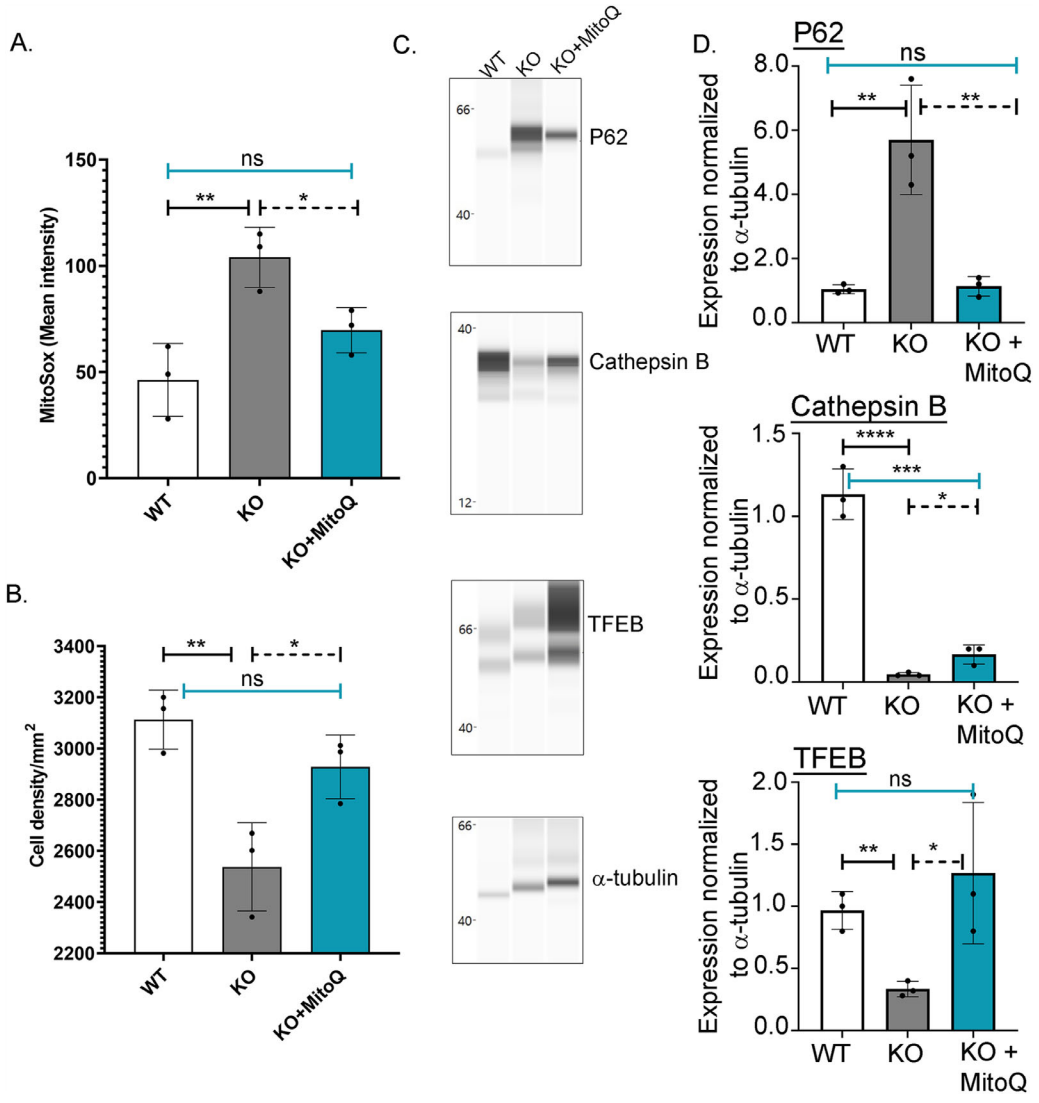

Figure 7. MitoQ in vivo reduces mitoROS, decreases cell loss, and improves lysosome protein expression in CHED mice. Intraperitoneal injections of MitoQ (68 µg) on alternate days starting at 8 weeks of age for 4 weeks. (**A**) MitoSox fluorescence intensity in corneal endothelium of WT, KO, KO + MitoQ animals, $n = 3$. Two females and one male mice for each group was used for this assessment. (**B**) Corneal endothelial density, $n = 3$, two female mice and one male mouse from each group. (**C**) Wes immunoassay of P62, Cathepsin B, and TFEB from *Slc4a11* WT and KO animals, two female mice of each group, repeated three times ($n = 2$ animals per group for each of the 3 trials). (**D**) Quantification of panel **C** data, mean ± SD, $^{*}P < 0.05$, $^{**}P < 0.01$, $^{***}P < 0.001$, $^{****}P < 0.0001$ (1-way ANOVA with Tukey's multiple comparisons test).

determine if MitoQ could reverse the in vivo disease phenotype, we conducted intraperitoneal injections of 68 µg MitoQ on 8-week-old *Slc4a11* KO mice on alternate days for 4 weeks. No significant changes in weight were noted in the animals during the course of the treatment (WT 22.3 ± 3.2 g, KO 23.4 ± 4.7 g, and KO + MitoQ 22.1 ± 3.9 g). At the end of the treatment duration, animals were euthanized, and the corneas were stained with MitoSOX Red on the endothelial side to detect the levels of mitochondrial ROS. Significant reduction of mitochondrial superoxide was detected in the corneal endothelium of KO animals injected with MitoQ when compared to KO animals injected with saline (Fig. 7A). DAPI staining of the corneal cups were conducted to determine corneal endothelial cell density. We also found that the endothelial cell density of non-treated KO mice was approximately 80% of that of WT animals, whereas with MitoQ injections, endothelial cell loss was 93% of WT levels (Fig. 7B).

We next determined whether MitoQ injection improved autophagy and lysosomal protein expression in *Slc4a11* KO animals. Corneal endothelium dissected from MitoQ treated KO animals showed improvement in both Cathepsin B and TFEB levels (Figs. 7C, 7D). Because of the small tissue size, cell fractionation using mouse corneal endothelial tissues is not feasible. TFEB is known to regulate its own transcription.[28] We therefore rationalized that a change in total TFEB levels indicates changes in its nuclear translocation. P62 levels were decreased in these animals when compared to KO control animals (see Figs. 7C, 7D).

Last, MitoQ injections resulted in significant reduction in corneal edema in *Slc4a11* KO animals (Figs. 8A, 8B).

Investigative Ophthalmology & Visual Science

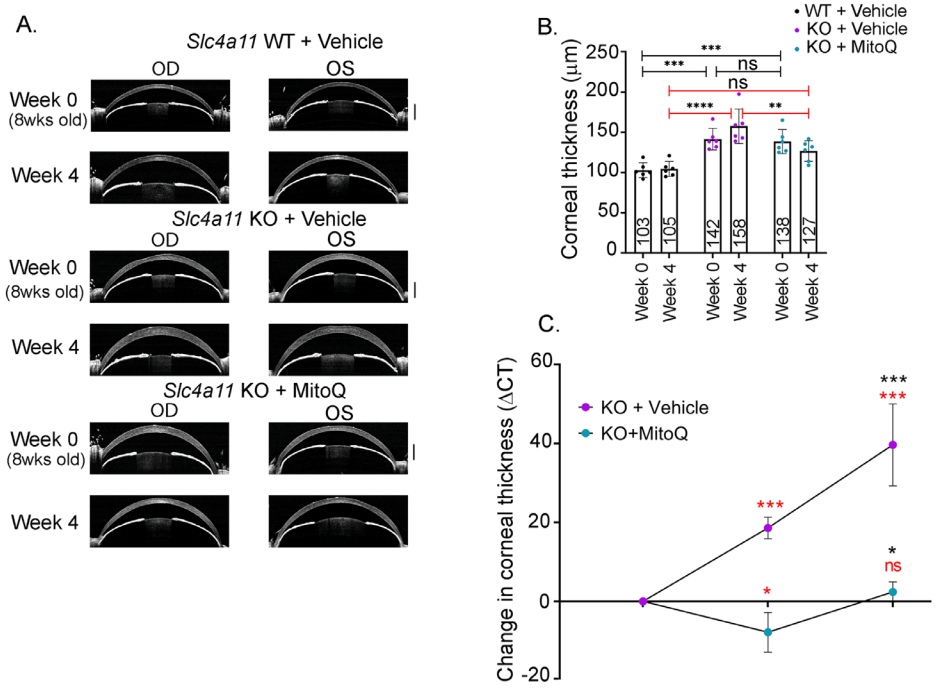

Figure 8. MitoQ in vivo reduces corneal edema in a mouse model of CHED. (**A**) Optical coherence tomography (OCT) images of *Slc4a11* WT and KO mouse corneas. Scale bar- 250 µm. (**B**) Quantification of change in corneal thickness from panel **A**. Mean corneal thickness is indicated inside the bar. (**C**) *Slc4a11* KO animals were injected either with MitoQ or vehicle for 2 weeks. Both groups of animals were left without any injections for another 2 weeks. Changes in corneal thickness measurements are plotted. *Red asterisks* denote the statistical significance when compared to week 0, *black asterisks* denote the statistical significance when compared to week 2. *$P < 0.05$, ***$P < 0.001$, ns = no significance, mean ± SD (1-way ANOVA with Tukey's multiple comparisons test).

Corneal edema progressed in vehicle injected KO animals and remained relatively unchanged in the WT animals (see Figs. 8A, 8B). To determine the specificity of MitoQ in reducing corneal edema, we conducted an additional experiment. Here, MitoQ was injected into a group of KO animals, whereas the littermates were not injected. Both groups had comparable corneal thickness at week 0. Two weeks after the injections, MitoQ treatment group showed a slight decrease in corneal thickness ($\Delta Ct = -8$ µm) while the control animals showed increased corneal thickness ($\Delta Ct = +19$ µm). At this point, the injections were stopped. OCT measurements were made 2 weeks later. The MitoQ injected group now had a slightly elevated $\Delta Ct = +2$ µm (compared to week 0). When compared to week 2, the MitoQ injected animals had a significant elevation in their corneal thickness (Fig. 8C, Supplementary Fig. S5). Thickness continued to progress in the non-injected group ($\Delta Ct = +40$ µm; see Fig. 8C, Supplementary Fig. S5). This reversal in the change of corneal thickness validates the effect of MitoQ.

Discussion

Here, we show that loss of *Slc4a11*, which leads to excessive glutamine dependent mitoROS, interferes with TFEB nuclear translocation, and lysosomal biogenesis and function, resulting in aberrant autophagy. Quenching of mitoROS by MitoQ rescues each of these parameters both in vitro and in vivo, resulting in a partial reversal of corneal edema in the mouse model of CHED. This is consistent with a previous study that showed partial alleviation of corneal edema in the CHED mouse when mitoROS was reduced by bypassing glutamine catabolism with dimethyl-α-ketoglutarate eye drops.[6] Taken together, these results confirm that excessive mitochondrial derived ROS drives the disease phenotype in CHED.

Corneal endothelial cell dysfunction, as evidenced by corneal edema, is apparent at eye opening in the CHED mouse. Whereas cell morphology is altered, cell density is not significantly different from WT at 10 weeks of age.[15] Significant reduction in cell density is noted in KO at 40 weeks of age.[15] Therefore, we set out to determine if enhanced autophagy slows cell death in these early stages. However, we found that mitochondrial ROS impedes lysosomal function and autophagy in *Slc4a11* KO corneal endothelial cells. In the KO cells, we observed modest upregulation of several autophagy associated proteins, however, autophagy flux was aberrant. In order for efficient degradation of substrates in the autophagosomes, normal activity of the lysosomal system is crucial. Therefore, we analyzed whether lysosomes are functional in *Slc4a11* KO cells. Lysosomal mass was decreased and lysosomal pH was increased in these cells. Most importantly, nuclear translocation of the master regulator of lysosomal function and biogenesis, TFEB was decreased. All these data indicate that autophagy, which in many cells enhance survival, is compromised in *Slc4a11* KO cells.

Inter-organelle communication has been recognized to be an essential component for normal cellular physiology.[33] Mitochondria-lysosome cross-talk is well studied in this regard. Loss of mitochondrial function in many cases impairs lysosomal activities.[34,35] This sometimes leads to decreased p-mTOR/mTOR ratio that reduces TFEB phosphorylation and increases nuclear translocation, which enhances lysosomal biogenesis.[33,36] This mechanism of action is evident in several cell types during acute mitochondrial stress but

not during chronic stress.[36] However, in the *Slc4a11* KO cells, a reduction in TFEB levels and activities, rather than an increase, was observed. These data suggest that chronic mitochondrial stress in *Slc4a11* KO cells may prevent TFEB translocation, which disrupts lysosome functions. Paradoxically, acute application of MitoQ in WT cells, while not producing a detectable change in MitoROS level (see Supplementary Fig. S4), decreased TFEB nuclear localization, lysosomal content and acidification. This suggests that some small amount of mitochondrial ROS, which we could not detect, may play a role in normal lysosomal biogenesis and function[36] or there is an off target effect of MitoQ.

Phosphorylation by mTOR prevents TFEB nuclear translocation, and thereby inhibits its transcriptional activities.[28,37] In the present study, nuclear levels of TFEB were decreased even with low pmTOR/mTOR ratio in *Slc4a11* KO cells, suggesting alternate mechanisms of TFEB regulation in these cells. Protein kinase B regulates TFEB through mTOR independent mechanisms,[38] and protein kinase C mediated inactivation of Glycogen Synthase Kinase β (GSK3β) is known to improve TFEB nuclear translocation.[39] In certain cell types during chronic stress conditions, the status of mTOR activation is not sufficient to enhance TFEB activities,[33,35,36] and it is stipulated that, in such situations, cells may conserve the limited functionality of damaged organelles rather than spend energy to recycle materials.[35] Whether chronic oxidative stress in *Slc4a11* KO cells supersedes mTOR regulation of TFEB will require additional studies.

Loss of lysosomal proteolytic activities compromise protein degradation pathways in many neurodegenerative diseases, such as Parkinson's disease, Alzheimer's disease, and amyotrophic lateral sclerosis.[40–42] In addition, impediments in autophagy due to lysosome dysfunctions are present in several ocular diseases, including glaucoma,[43] retinitis pigmentosa,[44] age related macular degeneration,[45] and granular corneal dystrophy.[46] To the best of our knowledge, the present study is the first to identify and characterize autophagy impairment and lysosomal malfunctions in CHED. Several studies have identified mitochondrial dysfunction, or oxidative stress as the trigger behind cell death in FECD, CHED, keratoconus, and granular corneal dystrophy.[4,5,47–50] Here, we further characterize the crosstalk between mitochondria and lysosomes in the corneal endothelial cells, and reveal that an important physiological process (autophagy) is disabled by increased mitochondrial ROS.

CHED is a disease with no cure. The prevalent form of treatment involves endothelial keratoplasty, an invasive procedure with significant risk of graft rejection. Our study shows that the use of a mitochondrial ROS quencher, MitoQ, can decrease endothelial cell loss and corneal edema in a mouse model of CHED. In the *Slc4a11* KO animal model, corneal edema precedes endothelial cell loss, indicating that cell function and not cell loss is the cause of the initial edema. However, with increasing age a continued increase in corneal edema is observed as well as a significant endothelial cell loss. At some point, cell loss will contribute to edema. MitoQ treatment reversed both corneal edema and endothelial cell loss in *Slc4a11* KO animals. We associate the edema reversal to rescue of cell function. Moreover, there is rescue of cell loss because both edema and cell loss are ameliorated by the decreased mitoROS levels. Animal studies involving type 2 diabetes,[32] kidney disease,[51,52] and sensorineural hearing loss[53] have shown promising results using MitoQ as a therapeutic agent. MitoQ was initially synthesized as a lipophilic molecule capable of specifically accumulating in the mitochondria.[54] It was used toward rescuing mitochondrial dysfunction in Parkinson's disease,[55] although clinical trials were ultimately unsuccessful, possibly because damage was already too extensive.[55] However, no major side effects were seen when given the maximum oral dose of MitoQ (80 mg/day) for a year, indicating that it was well tolerated.[55] Because repurposing of old drugs can circumvent many years of additional research that may go into the development of a new drug, MitoQ stands as a promising candidate toward the treatment of disease, such as CHED.

Acknowledgments

The authors thank Shimin Li for plasmid purification of GFP-LC3-RFP-LC3ΔG and Edward Kim for excellent technical assistance. Christiane Hassel, Indiana University Flow Cytometry Core Facility; Nuno Raimundo (Pennsylvania State University) for helpful critiques, Mallika Valapala (Indiana University Bloomington) for helpful suggestions toward experimental design, interpretation of results, and critical reading of the manuscript; and Catherine Cheng (Indiana University Bloomington) for the use of the Protein Simple Wes machine, the Zeiss LSM800 Confocal microscope, and critical reading of the manuscript.

Supported by - R01EY031321 and R01EY008834 to J.A.B., NIH/NCATS CTSI TL1 TR002531 and UL1 TR002529 (2018-2020) and Knights Templar Eye Foundation career starter grant (2019-2021) to R.S.

Disclosure: **R. Shyam**, None; **D.G. Ogando**, None; **M. Choi**, None; **P.B. Liton**, None; **J.A. Bonanno**, None

References

1. Bonanno JA. Molecular mechanisms underlying the corneal endothelial pump. *Exp Eye Res*. 2012;95(1):2–7.
2. Joyce NC. Proliferative capacity of corneal endothelial cells. *Exp Eye Res*. 2012;95(1):16–23.
3. Li S, Kim E, Bonanno JA. Fluid transport by the cornea endothelium is dependent on buffering lactic acid efflux. *Am J Physiol Physiol*. 2016;311(1):C116–C126.
4. Jurkunas U V., Bitar MS, Funaki T, Azizi B. Evidence of Oxidative Stress in the Pathogenesis of Fuchs Endothelial Corneal Dystrophy. *Am J Pathol*. 2010;177(5):2278–2289.
5. Katikireddy KR, White TL, Miyajima T, et al. NQO1 downregulation potentiates menadione-induced endothelial-mesenchymal transition during rosette formation in Fuchs endothelial corneal dystrophy. *Free Radic Biol Med*. 2018;116:19–30.
6. Ogando DGDG, Choi M, Shyam R, Li S, Bonanno JAJA. Ammonia sensitive SLC4A11 mitochondrial uncoupling reduces glutamine induced oxidative stress. *Redox Biol*. 2019;26:101260.
7. Guha S, Chaurasia S, Ramachandran C, Roy S. SLC4A11 depletion impairs NRF2 mediated antioxidant signaling and increases reactive oxygen species in human corneal endothelial cells during oxidative stress. *Sci Rep*. 2017;7(1):4074.
8. Aldave AJ, Han J, Frausto RF. Genetics of the corneal endothelial dystrophies: an evidence-based review. *Clin Genet*. 2013;84(2):109–119.
9. Schmedt T, Silva MM, Ziaei A, et al. Molecular bases of corneal endothelial dystrophies. *Am J Pathol*. 2010;95(5):24–34.

10. Zhang J, McGhee CNJ, Patel D V. The Molecular Basis of Fuchs' Endothelial Corneal Dystrophy. *Mol Diagn Ther*. 2019;23(1):97–112.
11. Loganathan SK, Schneider H-P, Morgan PE, Deitmer JW, Casey JR. Functional assessment of SLC4A11, an integral membrane protein mutated in corneal dystrophies. *Am J Physiol Cell Physiol*. 2016;311(5):C735–C748.
12. Malhotra D, Jung M, Fecher-Trost C, et al. Defective cell adhesion function of solute transporter, SLC4A11, in endothelial corneal dystrophies. *Hum Mol Genet*. 2020;29(1):97–116, doi:10.1093/hmg/ddz259.
13. Vithana EN, Morgan PE, Ramprasad V, et al. SLC4A11 mutations in Fuchs endothelial corneal dystrophy. *Hum Mol Genet*. 2008;17(5):656–666.
14. Riazuddin SA, Vithana EN, Seet L-F, et al. Missense mutations in the sodium borate cotransporter SLC4A11 cause late-onset Fuchs corneal dystrophy. *Hum Mutat*. 2010;31(11):1261–1268.
15. Han SB, Ang H-P, Poh R, et al. Mice with a targeted disruption of Slc4a11 model the progressive corneal changes of congenital hereditary endothelial dystrophy. *Invest Ophthalmol Vis Sci*. 2013;54(9):6179–6189.
16. Vithana EN, Morgan P, Sundaresan P, et al. Mutations in sodium-borate cotransporter SLC4A11 cause recessive congenital hereditary endothelial dystrophy (CHED2). *Nat Genet*. 2006;38(7):755–757.
17. Lee J, Giordano S, Zhang J. Autophagy, mitochondria and oxidative stress: cross-talk and redox signalling. *Biochem J*. 2012;441(2):523–540.
18. Zhang W, Ogando DG, Kim ET, et al. Conditionally Immortal Slc4a11-/- Mouse Corneal Endothelial Cell Line Recapitulates Disrupted Glutaminolysis Seen in Slc4a11-/- Mouse Model. *Invest Ophthalmol Vis Sci*. 2017;58(9):3723–3731.
19. Vilas GL, Loganathan SK, Liu J, et al. Transmembrane water-flux through SLC4A11: A route defective in genetic corneal diseases. *Hum Mol Genet*. 2013;22(22):4579–4590.
20. Wiesner R, Scheller C, Krebs F, Wätzig H, Oltmann-Norden I. A comparative study of CE-SDS, SDS-PAGE, and Simple Western: Influences of sample preparation on molecular weight determination of proteins. *Electrophoresis*. 2021:42(3):206–218.
21. Cheng T, Ding S, Liu S, Li Y, Sun L. Human umbilical cord-derived mesenchymal stem cell therapy ameliorate lupus through increasing CD4+ T cell senescence via MiR-199a-5p/Sirt1/p53 axis. *Theranostics*. 2021;11(2):893–905.
22. Hughes RO, Bosanac T, Mao X, et al. Small Molecule SARM1 Inhibitors Recapitulate the SARM1$^{-/-}$ Phenotype and Allow Recovery of a Metastable Pool of Axons Fated to Degenerate. *Cell Rep*. 2021;34(1):108588.
23. Kaizuka T, Morishita H, Hama Y, et al. An Autophagic Flux Probe that Releases an Internal Control. *Mol Cell*. 2016;64(4):835–849.
24. Katunuma N. Posttranslational Processing and Modification of Cathepsins and Cystatins. *J Signal Transduct*. 2010;2010:1–8.
25. Mach L, Mort JS, Glössl J. Maturation of human procathepsin B. Proenzyme activation and proteolytic processing of the precursor to the mature proteinase, in vitro, are primarily unimolecular processes. *J Biol Chem*. 1994;269(17):13030–13035.
26. Settembre C, Di Malta C, Polito VA, et al. TFEB Links Autophagy to Lysosomal Biogenesis. *Science (80-)*. 2011;332(6036):1429–1433.
27. Settembre C, Zoncu R, Medina DL, et al. A lysosome-to-nucleus signalling mechanism senses and regulates the lysosome via mTOR and TFEB. *EMBO J*. 2012;31(5):1095–1108.
28. Napolitano G, Ballabio A. TFEB at a glance. *J Cell Sci*. 2016;129(13):2475–2481.
29. Sardiello M, Palmieri M, di Ronza A, et al. A Gene Network Regulating Lysosomal Biogenesis and Function. *Science (80-)*. 2009;325(5939):473–477.
30. Palmieri M, Impey S, Kang H, et al. Characterization of the CLEAR network reveals an integrated control of cellular clearance pathways. *Hum Mol Genet*. 2011;20(19):3852–3866.
31. Oyewole AO, Birch-Machin MA. Mitochondria-targeted antioxidants. *FASEB J*. 2015;29(12):4766–4771.
32. Escribano-Lopez I, Diaz-Morales N, Rovira-Llopis S, et al. The mitochondria-targeted antioxidant MitoQ modulates oxidative stress, inflammation and leukocyte-endothelium interactions in leukocytes isolated from type 2 diabetic patients. *Redox Biol*. 2016;10:200–205.
33. Deus CM, Yambire KF, Oliveira PJ, Raimundo N. Mitochondria–Lysosome Crosstalk: From Physiology to Neurodegeneration. *Trends Mol Med*. 2020;26(1):71–88.
34. Baixauli F, Acín-Pérez R, Villarroya-Beltrí C, et al. Mitochondrial Respiration Controls Lysosomal Function during Inflammatory T Cell Responses. *Cell Metab*. 2015;22(3):485–498.
35. Fernandez-Mosquera L, Yambire KF, Couto R, et al. Mitochondrial respiratory chain deficiency inhibits lysosomal hydrolysis. *Autophagy*. 2019;15(9):1572–1591.
36. Fernández-Mosquera L, Diogo CV, Yambire KF, et al. Acute and chronic mitochondrial respiratory chain deficiency differentially regulate lysosomal biogenesis. *Sci Rep*. 2017;7(1):45076.
37. Martina JA, Chen Y, Gucek M, Puertollano R. MTORC1 functions as a transcriptional regulator of autophagy by preventing nuclear transport of TFEB. *Autophagy*. 2012;8(6):903–914.
38. Porter KM, Jeyabalan N, Liton PB. MTOR-independent induction of autophagy in trabecular meshwork cells subjected to biaxial stretch. *Biochim Biophys Acta - Mol Cell Res*. 2014;1843(6):1054–1062.
39. Li Y, Xu M, Ding X, et al. Protein kinase C controls lysosome biogenesis independently of mTORC1. *Nat Cell Biol*. 2016;18(10):1065–1077.
40. Rajawat YS, Hilioti Z, Bossis I. Aging: Central role for autophagy and the lysosomal degradative system. *Ageing Res Rev*. 2009;8(3):199–213.
41. Martinez-Vicente M, Sovak G, Cuervo AM. Protein degradation and aging. *Exp Gerontol*. 2005;40(8-9):622–633.
42. Koh J-Y, Kim HN, Hwang JJ, Kim Y-H, Park SE. Lysosomal dysfunction in proteinopathic neurodegenerative disorders: possible therapeutic roles of cAMP and zinc. *Mol Brain*. 2019;12(1):18.
43. Porter K, Nallathambi J, Lin Y, Liton PB. Lysosomal basification and decreased autophagic flux in oxidatively stressed trabecular meshwork cells. *Autophagy*. 2013;9(4):581–594.
44. Rodríguez-Muela N, Hernández-Pinto AM, Serrano-Puebla A, et al. Lysosomal membrane permeabilization and autophagy blockade contribute to photoreceptor cell death in a mouse model of retinitis pigmentosa. *Cell Death Differ*. 2015;22(3):476–487.
45. Golestaneh N, Chu Y, Xiao Y-Y, Stoleru GL, Theos AC. Dysfunctional autophagy in RPE, a contributing factor in age-related macular degeneration. *Cell Death Dis*. 2018;8(1):e2537–e2537.
46. Choi S-I, Kim B-Y, Dadakhujaev S, et al. Impaired autophagy and delayed autophagic clearance of transforming growth factor β-induced protein (TGFBI) in granular corneal dystrophy type 2. *Autophagy*. 2012;8(12):1782–1797.
47. Nita M, Grzybowski A. The Role of the Reactive Oxygen Species and Oxidative Stress in the Pathomechanism of the Age-Related Ocular Diseases and Other Pathologies of the

Investigative Ophthalmology & Visual Science

Anterior and Posterior Eye Segments in Adults. *Oxid Med Cell Longev*. 2016;2016:1–23.

48. Jurkunas U V., Rawe I, Bitar MS, et al. Decreased Expression of Peroxiredoxins in Fuchs' Endothelial Dystrophy. *Investig Opthalmol Vis Sci*. 2008;49(7):2956.
49. Wojcik K, Kaminska A, Blasiak J, Szaflik J, Szaflik J. Oxidative Stress in the Pathogenesis of Keratoconus and Fuchs Endothelial Corneal Dystrophy. *Int J Mol Sci*. 2013;14(9):19294–19308.
50. Atilano S, Lee D, Fukuhara P, et al. Corneal oxidative damage in keratoconus cells due to decreased oxidant elimination from modified expression levels of SOD enzymes, PRDX6, SCARA3, CPSF3, and FOXM1. *J Ophthalmic Vis Res*. 2019;14(1):62.
51. Xiao L, Xu X, Zhang F, et al. The mitochondria-targeted antioxidant MitoQ ameliorated tubular injury mediated by mitophagy in diabetic kidney disease via Nrf2/PINK1. *Redox Biol*. 2017;11:297–311.
52. Dare AJ, Bolton EA, Pettigrew GJ, Bradley JA, Saeb-Parsy K, Murphy MP. Protection against renal ischemia–reperfusion injury in vivo by the mitochondria targeted antioxidant MitoQ. *Redox Biol*. 2015;5:163–168.
53. Kim Y-R, Baek J-I, Kim SH, et al. Therapeutic potential of the mitochondria-targeted antioxidant MitoQ in mitochondrial-ROS induced sensorineural hearing loss caused by Idh2 deficiency. *Redox Biol*. 2019;20:544–555.
54. Kelso GF, Porteous CM, Coulter CV, et al. Selective Targeting of a Redox-active Ubiquinone to Mitochondria within Cells. *J Biol Chem*. 2001;276(7):4588–4596.
55. Snow BJ, Rolfe FL, Lockhart MM, et al. A double-blind, placebo-controlled study to assess the mitochondria-targeted antioxidant MitoQ as a disease-modifying therapy in Parkinson's disease. *Mov Disord*. 2010;25(11):1670–1674.

Investigative Ophthalmology & Visual Science